

Regular solutions in Abelian gauge model

Yuri N. Obukhov* and Franz E. Schunck

Institute for Theoretical Physics, University of Cologne, D-50923 Köln, Germany

()

Abstract

The regular solutions for the Ginzburg-Landau (-Nielsen-Olesen) Abelian gauge model are studied numerically. We consider the static isolated cylindrically symmetric configurations. The well known (Abrikosov) vortices, which present a particular example of such solutions, play an important role in the theory of type II superconductors and in the models of structure formation in the early universe. We find new regular static isolated cylindrically symmetric solutions which we call the type B and the flux tube solutions. In contrast to the pure vortex configurations which have finite energy, the new regular solutions possess a finite Gibbs free energy. The flux tubes appear to be energetically the most preferable configurations in the interval of external magnetic fields between the thermodynamic critical value H_c and the upper critical field H_{c2} , while the pure vortex dominate only between the lower critical field H_{c1} and H_c . Our conclusion is thus that type B and flux tube solutions are important new elements necessary for the correct understanding of a transition from the vortex state to the completely normal state.

*On leave from: Department of Theoretical Physics, Moscow State University, 117234 Moscow, Russia

PACS no.: 03.50.-z; 11.15.Kc; 74.20.De; 74.60.-w

Typeset using REV_T_EX

1. INTRODUCTION

The Ginzburg-Landau theory of superconductivity [1] is mathematically equivalent to the Abelian theory of coupled gauge and Higgs fields [2]. The existence of vortex (string-like) solutions in it was predicted by Abrikosov in 1952 (and published 5 years later [3]) in the context of the phenomenological model of superconductors and was discussed in [2] in the framework of the dual string approach (see also a recent generalization to the case of nontrivial helicity in [4]). The aim of this work is to clarify, with the help of the careful numerical analysis, the properties of such solutions and to construct new solutions. We confine ourselves to the case of cylindrical symmetry, thus considering an isolated vortex and related field configurations. In the literature devoted to this subject (see, e.g., [2,3,5–9]) main attention was paid to approximate solutions and qualitative methods, but there were very few attempts to study exact solutions by numerical methods. Moreover, as recently was shown in [10], the old qualitative results may contain mistakes and are incomplete. Approximate results are normally confined to the domains of very small ($\lambda \ll 1$) or extremely large ($\log \lambda \gg 1$) values of the coupling constant λ (or the characteristic Ginzburg-Landau parameter $\kappa = \sqrt{\lambda}$, see Appendix). As for numerical studies, one can mention the earlier reports [11–15] and more recent (variational) analysis in [16]. In our paper we present new numerical results for the isolated regular structures in the Ginzburg-Landau (-Nielsen-Olesen) model. Although here we confine ourselves to the case of Abelian gauge field, we will consider elsewhere the non-Abelian generalizations (cf. previous approaches in [17,18]). Our results demonstrate a rich structure of the space of exact solutions for the classical Ginzburg-Landau model. Besides the well known vortex solutions, for which we compute a variety of parameters in an interval of values of λ close to the critical value $\lambda = \frac{1}{2}$ ($\kappa = \sqrt{\frac{1}{2}}$), we describe some new exact regular solutions. In our opinion, of particular interest are the configurations which we call the *flux-tube* and the *oscillating* solutions below. The former appear to comprise a new nontrivial structure in ideal type II superconductors which is important for understanding the transition between a pure vortex state and a normal state.

As it is well known, the vortex (or the mixed) state of a type II superconductor exists between the critical magnetic fields H_{c_1} and H_{c_2} . Their values, as claimed in the literature [3,5–9], can be determined from the analysis of isolated vortex solutions. However, from our results we conclude that such a claim is correct only partly. Indeed, H_{c_1} is determined, for each value of $\lambda = \kappa^2$, by a relevant isolated vortex solution from a comparison of the Gibbs free energy of the vortex configuration with that of the pure Meissner configuration. But the upper critical magnetic field H_{c_2} appears to be completely unrelated to the vortex configurations. Instead, one can only determine H_{c_2} from a similar comparison of the Gibbs free energy for a normal state with that of a different type of exact regular solutions of the Ginzburg-Landau equations. We call these the type B solutions. Actually, *approximate* type B solutions are usually described in the literature [3,5–9] in the framework of analysis of the *linearized* Ginzburg-Landau equations. We construct numerically exact self-consistent type B solutions. Although interesting enough themselves as mathematical structures, the type B solutions have a limited physical value as compared to the new flux tube solutions. The latter configurations correctly describe the transition from a pure vortex to a normal state, as will be demonstrated below.

It seems worthwhile to notice that the Ginzburg-Landau equations describe common extremals for two different (action type) functionals: for the usual *energy* and for the *Gibbs free energy* integrals. The principal difference of the vortex and the new solutions is that the former are the *finite energy* configurations, while the latter are the *finite Gibbs free energy* configurations. Previously, attention in the literature was paid only to the finite energy regular solutions of the Ginzburg-Landau equations. In the context of cylindrical symmetry, these are the famous Abrikosov(-Nielsen-Olesen) vortices. It is our aim to demonstrate the existence and the physical relevance of two large families of *finite Gibbs free energy* regular solutions which are described in our paper as the the flux tube (or type A) and the type B solutions. In our opinion, the correct understanding of the mixed state of type II superconductor can only be achieved after taking into account these new solutions. In particular, it turns out that the class of the flux tube solutions is divided into an infinite number of

families labeled by a number of nodes n for the scalar field configuration. Each family exists on a finite interval of magnetic field (definition of limiting points see below). In this way, one finds a certain *fine structure of the mixed state* for an ideal type II superconductor.

The plan of the paper is as follows: Section 2 contains a general introduction to the model, we discuss the two energy functionals and formulate general regularity conditions at the origin. A brief account of numerical analysis of the pure vortex solutions is given in Section 3. Sections 4 and 5 contain the description of new solutions, the type B and the flux tubes, respectively. In Section 6 we perform the linearization analysis of the Ginzburg-Landau equations, while Section 7 is devoted to the regular oscillating solutions. The latter appear to be certain unstable “relatives” of the vortices. Finally, Section 8 contains a short discussion and a summary of the results obtained. In the Appendix we compare our notations and conventions with the old ones used in the literature. A general remark is necessary for the tabulated matter: We find it impossible to include all the available numerical data into the Tables which contain only some selected reasonable minimum of data. The Figures present additional information.

2. ENERGY FUNCTIONALS AND REGULARITY CONDITIONS

A. Nielsen-Olesen Lagrangian

The Lagrangian of the Abelian (“Nielsen-Olesen” [2]) gauge model describing interacting electromagnetic $F = dA$ and complex scalar field Φ reads

$$L_{\text{NO}} = -\frac{1}{2}(F \wedge {}^*F + D\Phi \wedge {}^*\overline{D\Phi}) - \mathcal{V}(|\Phi|)\eta, \quad (2.1)$$

with the potential

$$\mathcal{V}(|\Phi|) = \frac{\lambda}{4} \left(|\Phi|^2 - \frac{\mu^2}{\lambda} \right)^2, \quad (2.2)$$

where the overbar denotes complex conjugation and $D = d + iA$, and star * is the Hodge dual operator, $\eta := {}^*1$ being the volume form.

Noticing that μ has a dimension of inverse length, we can introduce for the cylindrical system (ρ, θ, z) a new (dimensionless) radial coordinate r via $\rho = \frac{\sqrt{\lambda}}{\mu}r$. We are looking for *static* configurations, and use the following cylindrically symmetric ansatz (cf. [2])

$$A = f(r)d\theta, \quad \Phi = \frac{\mu}{\sqrt{\lambda}}\varphi(r), \quad (2.3)$$

where f, φ are two *real* functions.

The magnetic field 1-form, defined as the (three-dimensional) Hodge dual *F , has only one component in z -direction, ${}^*F = Hdz$, where the latter is given by the expression

$$H = \frac{\mu^2}{\lambda} \frac{1}{r} \frac{df}{dr}. \quad (2.4)$$

We will denote the *dimensionless* magnetic field by $h := H\lambda/\mu^2 = f'/r$.

Magnetic field is conveniently characterized by the flux it produces through a two-dimensional surface. In a cylindrically symmetric case the total flux over a surface orthogonal to the z -axis is

$$F = \int \rho d\rho d\theta H = 2\pi \int_0^\infty dr \frac{df}{dr} = 2\pi[f(\infty) - f(0)]. \quad (2.5)$$

B. Energy (line density) functional and equations of motion

For the Lagrangian (2.1) one can immediately write the energy per unit length in the form

$$\mathcal{E} = \frac{2\pi\mu^2}{\lambda} \int_0^\infty dr r \frac{1}{2} \left[\left(\frac{1}{r} \frac{df}{dr} \right)^2 + \left(\frac{d\varphi}{dr} \right)^2 + \frac{1}{r^2} f^2 \varphi^2 + \frac{\lambda}{2} (\varphi^2 - 1)^2 \right]. \quad (2.6)$$

Notice that it is not necessary to include a phase factor $e^{in\theta}$ for the scalar field in the ansatz (2.3), as it is done in a number of different approaches. The field φ is always defined up to a gauge transformation and we find it more convenient to work in the gauge (2.3).

Now, it is straightforward to see that the equations of motion of the Nielsen-Olesen model [2] read:

$$r^2 f'' - r f' = r^2 \varphi^2 f, \quad (2.7)$$

$$r^2 \varphi'' + r \varphi' = \varphi(f^2 + \lambda r^2(\varphi^2 - 1)). \quad (2.8)$$

The value of the constant λ plays an important role. If it equals to the critical value $\lambda = \frac{1}{2}$, the Nielsen-Olesen equations are consequences of the *first order* (Bogomolny) system

$$\frac{1}{r} f' + \frac{1}{2}(\varphi^2 - 1) = 0, \quad (2.9)$$

$$\varphi' + \frac{1}{r} f \varphi = 0. \quad (2.10)$$

In the theory of superconductivity $\lambda = \frac{1}{2}$ separates two phases: for $\lambda > \frac{1}{2}$ (resp., $\lambda < \frac{1}{2}$) one has a type II (resp., type I) superconductor. The critical subcase was extensively studied in the literature [19–21,16]. The general noncritical case for $\lambda \neq \frac{1}{2}$ is much less investigated.

Using (2.4), we can write the equation (2.7) in the form

$$h' = \frac{1}{r} f \varphi^2, \quad (2.11)$$

and hence the system (2.7)-(2.8) can be transformed into

$$h'' + \frac{1}{r} h' = h \varphi^2 + 2h' \frac{\varphi'}{\varphi}, \quad (2.12)$$

$$\varphi'' + \frac{1}{r} \varphi' = \varphi \left(\frac{1}{\varphi^4} (h')^2 + \lambda(\varphi^2 - 1) \right), \quad (2.13)$$

explicitly for the coupled magnetic field h and scalar field φ variables. This system is however not particularly useful for numerical investigation because of explicit $1/\varphi$ terms.

C. Gibbs free energy functional

The line energy density functional (2.6) is minimal ($\mathcal{E}_{min} = 0$) for the Meissner state, i.e., when $\varphi = 1$ (superconducting order in all points of a sample) and $h = 0$ (no magnetic field inside a superconductor). This corresponds to a trivial solution of (2.7)-(2.8), $f = 0, \varphi = 1$. The normal state is described by another simple solution, $f = C + \frac{1}{2}h_0 r^2, \varphi = 0$, (C and h_0 are constants), which always (with or without magnetic field h_0) has formally infinite energy \mathcal{E} . However physically, of interest is a difference of energies, not an energy itself.

In particular, let us turn our attention to the Gibbs free energy (per unit length) which is defined by

$$\mathcal{G} = \mathcal{E} - \int d^2x (\mathbf{H} \mathbf{H}_{\text{ext}}). \quad (2.14)$$

We assume that both magnetic fields, the internal one \mathbf{H} and an external \mathbf{H}_{ext} are directed along the z -axis, and use the dimensionless values of fields defined, in accordance with (2.4), by $H = (\mu^2/\lambda)h$ and $H_{\text{ext}} = (\mu^2/\lambda)h_{\text{ext}}$. The Gibbs free energy of the normal state with a magnetic field $h_0 = h_{\text{ext}}$ is given by the integral

$$\mathcal{G}_{nh} = \mathcal{E}[\varphi = 0, h = h_0] - \frac{2\pi\mu^2}{\lambda} \int_0^\infty dr r h_0 h_{\text{ext}} = \frac{2\pi\mu^2}{\lambda} \int_0^\infty dr r \frac{1}{2} \left[-h_0^2 + \frac{\lambda}{2} \right]. \quad (2.15)$$

For a sample without boundary, this is an infinite constant, while for a cylinder of a radius R this is a finite positive (negative) constant $\pi R^2 \mu^2 (1/2 - h_0^2/\lambda)/2$ for a magnetic field $h_0 < h_c$ ($h_0 > h_c$), and zero for $h_0 = h_c := \sqrt{\lambda/2}$. This observation underlies the physical interpretation of h_c as a critical (so called thermodynamic) value of the magnetic field which distinguishes normal and superconducting phases.

However, let us consider the difference,

$$\begin{aligned} \Delta\mathcal{G} &:= \mathcal{G} - \mathcal{G}_{nh} \\ &= \frac{2\pi\mu^2}{\lambda} \int_0^\infty dr r \frac{1}{2} \left[\left(\frac{1}{r} \frac{df}{dr} - h_0 \right)^2 + \left(\frac{d\varphi}{dr} \right)^2 + \frac{1}{r^2} f^2 \varphi^2 + \frac{\lambda}{2} (\varphi^4 - 2\varphi^2) \right]. \end{aligned} \quad (2.16)$$

It is very important to notice that the Gibbs functional (2.16) has the *same equations for extremals* as the energy functional (2.6), namely (2.7)-(2.8). However, unlike the strictly positive (2.6), the functional (2.16) can have any sign.

D. Regularity at the symmetry axis

Looking for solutions which are regular at the origin, we substitute the series expansions

$$f = \sum_{k=0} a_k r^k, \quad \varphi = \sum_{k=0} b_k r^k, \quad (2.17)$$

into (2.7)-(2.8). We then find two types of conditions:

(A) Potential f is non-zero while scalar field φ vanishes at the origin,

$$f = N + ar^2 + \frac{1}{4N(N+1)}b^2 r^{2N+2} + O(r^{2N+4}), \quad (2.18)$$

$$\varphi = br^N \left(1 + \frac{N}{2(N+1)} \left(a - \frac{\lambda}{2N} \right) r^2 + O(r^4) \right), \quad (2.19)$$

where $N = \pm 1, \pm 2, \dots$ is a nonzero integer and parameters a, b are arbitrary.

(B) Potential f vanishes while scalar field φ is nontrivial at the origin,

$$f = ar^2 \left(1 + \frac{1}{8}b^2 r^2 + O(r^4) \right), \quad (2.20)$$

$$\varphi = b \left(1 + \frac{\lambda}{4}(b^2 - 1)r^2 + O(r^4) \right), \quad (2.21)$$

with some parameters a, b .

In both cases, parameter a determines the value of the magnetic field at the origin, $h(0) = 2a$. When $b = 0$, both cases reduce to the solution which describes a normal superconductor $\varphi = 0$ filled by the constant homogeneous magnetic field $h(r) = h(0) = 2a$.

3. VORTEX SOLUTIONS

Vortex solutions of the Ginzburg-Landau equations (2.7)-(2.8) are distinguished among others by the special conditions at infinity which read:

$$f(r)|_{r \rightarrow \infty} \longrightarrow 0, \quad (3.1)$$

$$\varphi(r)|_{r \rightarrow \infty} \longrightarrow 1. \quad (3.2)$$

When combined with the type A regularity conditions at the origin (2.18)-(2.19), these asymptotic conditions define uniquely parameters a, b for any value of λ and N . The meaning of the constant N is clear: this is the value of the magnetic flux described by such solutions. Indeed, we substitute $f(0) = N$ and $f(\infty) = 0$ into (2.5) to obtain $F = -2\pi N$. This is the well known flux quantization result for superconductors. Notice that the asymptotics (3.1)-(3.2) cannot be realized for any solution with type B regularity conditions (2.20)-(2.21), see the discussion in the next section.

The results of the numerical integration are given in Figures 1, 2 and Table I, where left and right columns describe solutions for $N = 1$ and $N = 2$, respectively. For convenience of comparison with the old calculations [11–15] we write the coupling constant as $\lambda = \kappa^2$ [see Appendix for definitions, in particular (A.5)].

Energy (2.6) is always positive on all vortex configurations, cf. Fig. 3. It decreases with growing κ and increases when $\kappa \rightarrow 0$. A useful physical variable, which allows to find necessary conditions for the existence of vortices, is the Gibbs free energy (line density) (2.14). This quantity is zero for the Meissner state ($h = 0, \varphi = 1$), while for a vortex state it is always positive when an external magnetic field \mathbf{H}_{ext} is oriented oppositely to the magnetic field \mathbf{H} inside a sample (hence such vortices are ruled out), and it can become negative for a certain value of external field with the same orientation as in the sample. In the latter case, for a constant external magnetic field $\mathbf{H}_{\text{ext}} = (0, 0, H_{\text{ext}})$ one finds

$$\mathcal{G} = \mathcal{E} - 2\pi H_{\text{ext}} \left| \int_0^\infty dr r h \right| = \mathcal{E} - 2\pi |N| H_{\text{ext}}. \quad (3.3)$$

Hence the lower critical value of an external magnetic field $H_{\text{ext}} = H_{c1}$, determined by the condition $\mathcal{G} = 0$, is equal to

$$H_{c1} = \frac{\mathcal{E}}{2\pi|N|} = \frac{\kappa\epsilon}{4\pi|N|}\sqrt{2}H_c, \quad (3.4)$$

where in the last equality we switched to the old conventions summarized in Appendix.

It seems worthwhile to make the following short remark: The analysis of exact vortex configurations reveals a disagreement with the numerous claims in the literature (see, e.g., [5–7,9]) concerning a possible qualitative (and to some extent a quantitative) understanding of these solutions on the basis of so called penetration lengths for the magnetic and the scalar fields. As we recall in the Appendix, the (formally derivable from the microscopic theory) magnetic penetration length δ and scalar field coherence length ξ are related to the coupling parameter via the formula (A.2). Using that relation, it is common to claim that for large κ the domain of a magnetic field penetration is greater than a domain of essential change of scalar field, while for small κ the opposite is true. Our comparison of the *actual*

(computed for vortices) penetration lengths for different values of κ demonstrates that the domain of the magnetic field penetration is *always* greater than the domain of an essential change of the scalar field, even for small κ , see Fig. 4. In fact, this observation was also confirmed in earlier numerical studies, [12,11].

4. REGULAR SOLUTIONS FOR TYPE B CONDITIONS

The type B conditions (2.20)-(2.21), like the type A conditions (2.18)-(2.19), guarantee a regular behavior of solutions at the origin. (It seems worthwhile to notice that type B conditions are *not* a particular case of type A for $N = 0$). It is straightforward to analyze a qualitative behavior of such solutions for finite values of r . For example, equation (2.7) immediately yields that $f(r)$ is a monotonous increasing for $a > 0$ (decreasing for $a < 0$) function. Indeed, if we assume an extremum for a finite $r = r_0$, one finds from (2.7) $f''(r_0) = \varphi^2 f(r_0)$ which means that such an extremum is a minimum for positive $f(r_0)$ and a maximum for negative $f(r_0)$. For a function starting from a zero (2.20) both possibilities are excluded and thus $f(r)$ is a monotonous function. In particular, this means that $f(r) \rightarrow \infty$ for $r \rightarrow \infty$, and one thus concludes that *no finite energy* solutions for type B regularity conditions exist: the functional (2.6) is infinite.

Let us however look at (2.7)-(2.8) as the equations for extremals of the Gibbs free energy functional (2.16). It is immediately clear that there exist *finite Gibbs free energy* regular type B solutions, provided they satisfy at infinity

$$h(r) = \frac{1}{r} f'(r) \Big|_{r \rightarrow \infty} \longrightarrow h_0, \quad (4.1)$$

$$\varphi(r)|_{r \rightarrow \infty} \longrightarrow 0. \quad (4.2)$$

Notice that unlike in a vortex configuration (3.2), the scalar field cannot approach at infinity any finite value except 0.

The results of numerical integration are presented in Tables II-VI and Figures 5-9. A principal difference of these solutions (which we will call “type B” solutions for brevity) from

the vortex solutions lies in the fact that the magnetic field is asymptotically constant, and hence the flux integral defined by (2.5) is formally infinite. However a reasonable replacement is provided by the quantity

$$M := \Delta F = \int \rho \, d\rho \, d\theta \, (H - H_0) = 2\pi \int_0^\infty dr \, r \, (h - h_0). \quad (4.3)$$

Defined formally as a difference of fluxes, this variable is usually interpreted as a *magnetization* per unit volume [7,13]. Unlike the quantized flux for the vortices, M can have an arbitrary value.

From Tables III-VI we see, for the type B solutions without node, that when $a \rightarrow \lambda/2$ the external magnetic field is approaching $h_{\text{ext}} = h_{c_2} = \lambda$, while $M/(2\pi) = \Delta\mathcal{G} = 0$. For $\lambda > 1/2$ (Tables IV-VI), we find a higher external magnetic field for larger values of magnetic field at the center $h(0) = 2a$. When $\lambda = 1/2$, for all solutions $h_{\text{ext}} = 1/2$ (Table II). Finally, for $\lambda < 1/2$ (Table III) the external magnetic field is decreasing when $h(0) = 2a$ grows (the reverse order as compared to the $\lambda > 1/2$ case).

Besides the simple type B solutions without nodes (displayed on Figures 5, 6), there exist more nontrivial solutions with nodes. Configurations with one node are represented by the right columns in the Tables III-VI and are shown on Figures 8, 9.

For $\lambda > 1/2$ all type B solutions without node have a negative Gibbs free energy $\Delta\mathcal{G}$, for $\lambda = 1/2$ always $\Delta\mathcal{G} = 0$, and for $\lambda < 1/2$ the Gibbs free energy is positive. One can find also negative $\Delta\mathcal{G}$ for type B solutions with one node when $h_c < \lambda/3$ (i.e., $\kappa > 3/\sqrt{2}$), see the case of $\kappa = 2.25$ (Table VI). This will be clarified later in Section 6.

The magnetization curves for the type B solutions are given in Figure 15. For any $\lambda = \kappa^2$, M diverges at h_c .

5. FLUX TUBE SOLUTIONS

Let us look for the other solutions which yield finite values for the Gibbs functional (2.16). At the origin $r = 0$ we take the type A regularity conditions (2.18)-(2.19), while at

infinity we consider the asymptotics (4.1)-(4.2). Such a combination of two type conditions at zero and at infinity suggests a possible physical interpretation of such solutions which appear as a result of a certain “gluing” of a vortex configuration at the origin with a type B solutions at large radial values.

The results of numerical integration are given in Figures 10-21 and Tables VII-XI (without nodes) and Tables XII-XIV (with one node). As in the previous section, we present results only for the values of $\kappa = 0.5, 1.0, 1.5, 2.25, 5.0$.

Figures 10-14 explain why we call these solutions the *flux tubes*: There is a core where matter is in a state close to the normal one filled by the magnetic field (this is in fact a vortex), surrounded by a superconducting tube (almost completely free of a magnetic field). Outside such a tube the sample quickly reduces to a normal state with the external field penetrated in it. For the solutions with one node we have a “sandwich-like” structure: a tube of normal state between two superconducting tubes, see Fig. 14.

Each family of flux tube solutions has two branches. E.g., for $\kappa = 1$, one of these branches is characterized by the positive Gibbs free energy, and another has negative Gibbs free energy. However, for sufficiently large κ both branches describe the negative Gibbs free energy configurations. We find it convenient to depict these branches in the form of magnetization curves, Figure 16. For $\lambda \leq \frac{1}{2}$, two branches with positive Gibbs free energy exist. As in the case of type B solutions, M diverges at h_c .

It is interesting to notice that among the flux tube configurations there are solutions with quite unusual behavior of the magnetic field, which in the center is oppositely oriented with respect to the direction of external magnetic field. See the data with negative a in the Tables VIII-XI (notice that for $\kappa = 2.25$ and $\kappa = 5.0$ there exist negative Gibbs free energy solutions with such property).

Like for the type B configurations, we also find the flux tube solutions with one node, relevant data is displayed in Figure 14, 17-20 and Tables XII-XIV. Notice that for $\kappa = 1$ all the flux tube solutions with one node have positive Gibbs free energy. However, with increasing κ this changes. The important thing is the position of the thermodynamic critical

value h_c relative to the “limiting points” for h_{ext} of the flux tube families, at which the magnetization and the Gibbs free energy vanishes. We have determined numerically the values of such limiting points which depend on the value of κ and are located, on the h_{ext} axis, at $\lambda, \frac{1}{3}\lambda, \frac{1}{5}\lambda, \frac{1}{7}\lambda, \dots$. In the next section we explain the values of these limiting points with the help of linearization analysis.

The reader should compare the magnetization curve and the $(\Delta\mathcal{G}/h_{\text{ext}})$ energy/field plots for $\kappa = 1.0, 1.5, 2.25, 5.0$, Figures 16-20, which demonstrate that the “motion” of the limiting points to the right of h_c is accompanied by creation of flux tubes with one node which have negative Gibbs free energy.

Both, the type B solutions and the flux tube solutions, have a well defined Gibbs free energy for an infinite sample. It is natural to compare them. Of course, this must be done in a correct way: one should compare energies of configurations with the same values of external magnetic field h_{ext} . Using our data, we can display the Gibbs free energy $\Delta\mathcal{G}$ as a function of h_{ext} . These functions for the type B and the flux tubes are given on the Figures 18-20, showing that the flux tube configurations are energetically more preferable.

6. LINEARIZED SYSTEM AND CRITICAL MAGNETIC FIELDS

The best way to understand the structure of type B and flux tube solutions in the limit of vanishing magnetization $M \rightarrow 0$ and the Gibbs energy $\Delta\mathcal{G} \rightarrow 0$ is to study the linearized Ginzburg-Landau equations.

Let us consider, in the spirit of [3,5–9], the system (2.7)-(2.8) in the situation when the square of the scalar field φ^2 is negligibly small. Mathematically this means that, in the lowest order, one drops out the terms containing φ^2 in (2.7) and (2.8). We then immediately notice that such a linearized system

$$r^2 f'' - r f' = 0, \quad (6.1)$$

$$r^2 \varphi'' + r \varphi' = \varphi(f^2 - \lambda r^2), \quad (6.2)$$

is a consequence of any of the *first order* systems

$$\frac{1}{r}f' - s\lambda = 0, \quad (6.3)$$

$$\varphi' + s\frac{1}{r}f\varphi = 0, \quad (6.4)$$

where $s = \pm 1$ is the sign factor.

This system is straightforwardly integrated and yields

$$f(r) = N + s\frac{\lambda}{2}r^2, \quad (6.5)$$

$$\varphi(r) = \varphi_0 r^{-sN} \exp\left(-\frac{\lambda}{4}r^2\right), \quad (6.6)$$

where N and φ_0 are integration constants. In the linear approximation, the constant N is arbitrary, but as we can see from the analysis of the complete *self-consistent* system at the origin (2.18)-(2.21), this constant should be either 0 or $\pm 1, \pm 2, \dots$. In order to have a regular behavior of (6.6) at $r = 0$, one should choose the sign of N in such a way that $sN < 0$. Notice that the potential (6.5) describes an homogeneous constant magnetic field $h = s\lambda$, and thus the value of s shows its direction (up or down along the z axis).

It is easy to check that all the solutions (6.5) and (6.6), for arbitrary values of integration constants, have the same (zero) energy integral computed for the linearized system (6.1)-(6.2). For $N = 0$ the field (6.6) evidently describes the linearized type B solution, while for $N = 1$ this is a linearized flux tube solution. As we see, the linearized solutions are energetically equivalent. However, the numerical results (see Figures 18 and 19) definitely show that self-consistent flux tubes are energetically more preferable than the type B configurations.

The first correction to the magnetic field is easily computed. One must now take the complete system, and consider the first equation (2.7) in the form (2.11) where the right hand side is constructed from the lowest order configurations (6.5) and (6.6). Since these satisfy (6.4), we find from it $\frac{1}{r}f\varphi^2 = -\frac{1}{2}s(\varphi^2)'$, and hence (2.11) is immediately integrated, yielding for the magnetic field

$$h = s\left(\lambda - \frac{1}{2}\varphi^2\right). \quad (6.7)$$

As we see, an important role is played here by the normalization of the linearized solution, i.e. by the constant φ_0 .

Further insight can be obtained also directly from the analysis of the second order linearized system (6.1)-(6.2). Indeed, integration of (6.1) is straightforward, giving

$$f = N + \frac{h}{2}r^2, \quad (6.8)$$

where N and h are integration constants with the latter representing the value of an homogeneous constant magnetic field. After substituting (6.8) into (6.2) we find a Schrödinger type of equation for φ with the potential of a circular oscillator. Regular solutions exist only when

$$h = \frac{s\lambda}{1 + 2n + sN + |N|}, \quad (6.9)$$

where $n = 0, 1, 2, \dots$. Corresponding eigenfunctions $\varphi_{n,N}$ are given in terms of the Laguerre polynomials, with n equal to the number of zeros (nodes). Let us introduce the notation

$$h_k := \frac{\lambda}{2k+1}, \quad k = 0, 1, 2, \dots \quad (6.10)$$

It is easy to see that the maximal eigenvalue (6.9), $h = s\lambda = sh_0$, is achieved for $n = 0$ and $sN = -|N|$, and the scalar field is then described exactly by (6.6). This maximal eigenvalue is precisely the second critical field $h_{c2} = \lambda = \kappa^2$. The rest of eigenvalues also have clear physical meaning: these define the values of the external magnetic field at which the exact type B and flux tube solutions become “linearizable” and thus disappear. Looking at the Tables VII-XI, XII-XIV, II-VI, we find the complete agreement with the above linearization analysis. Indeed, the flux tube (without nodes) and the type B (without nodes) configurations have the limit magnetic field values $h_1 = \lambda/3$ and $h_0 = h_{c2}$, while the flux tubes and type B solutions with one-node “live” between $h_2 = \lambda/5$ and $h_1 = \lambda/3$. In general, the family of solutions with k nodes have the limiting points h_{k+1} and h_k . If h_c belongs to the interval $[h_{k+1}, h_k]$, then $h_{k+1} < h_{\text{ext}} < h_k$ for all solutions in this family. However when h_c does not belong to this interval, then $[h_{k+1}, h_k]$ is extended up to h_c .

This linearization analysis clearly supports the existence of the flux tube type solutions.

7. OSCILLATING SOLUTIONS

Let us now consider weaker conditions at infinity: potential still satisfy (3.1), however instead of (3.2) we require regularity and finiteness of the scalar field. From the physical interpretation of φ as the “density of superconducting electrons” one concludes that $|\varphi| < 1$ for all values of the radial coordinate r .

Qualitatively, one can understand the behavior of a scalar field for large r as follows. When in (2.8) the potential f^2 and the scalar field φ^2 nonlinear terms become small enough, one is left with the linearized equation

$$\varphi'' + \frac{1}{r}\varphi' + \lambda\varphi = 0, \quad (7.1)$$

which has the Bessel function as a solution $\varphi = J_0(\sqrt{\lambda}r) = J_0(\kappa r)$. Such an asymptotic behavior is confirmed by direct numerical integration, see Figures 22-24 and Table XV.

To the best of our knowledge, this type of solution was never reported in the literature. It is interesting to find out, what physics corresponds to it. We think these new oscillating solutions are unstable configurations preceding to the completely formed Abrikosov vortex state, they appear when the external magnetic field is switched on and reaches H_{c1} . We may draw attention to the following remarks in an experimental research paper: “Consistent values of the magnetization were obtained for fields just above H_{c1} only after the sample had been moved between the coils a number of times. The change in the magnetization of a sample upon a slight increase (or decrease) of the field is very dependent on the fact that the sample has been jarred as it is pulled between the measuring coils, and a final, steady-state value of the magnetization is sometimes obtained only after 10 or 20 sample translations. It is as if vibration assists the flux movement into or out of the sample. Hence, all of the data reported below refer to the final steady state of the magnetization; that is, further sample motion would produce no further change” [22].

For the *type A* conditions at the origin, the results of numerical integration are given in Table XV. In general, oscillating solutions exist only for initial values (a, b) below the ones

(a^*, b^*) of the vortex solution (first line of Table XV). The flux for the displayed solutions is always $F/(2\pi) = -1$. The values here are given for $\kappa = 1.0$. From Figure 22, one recognizes that for b close to b^* the scalar field reaches almost the value 1, i.e. a complete superconducting state.

Due to a not so quick decay of the scalar field at infinity, approximately $\varphi \sim \cos(\kappa r)/\sqrt{r}$, the energy of an oscillating solution is infinite for an infinite sample, but for a real finite cylindrical sample it is finite, although larger than the energy of a vortex configuration. Notice, that an oscillating character of such solutions may resemble an “intermediate” superconducting state with coexisting normal and superconducting regions [6]. However a considerable difference is that the magnetic field penetrates only at the center, exactly like in a vortex case. Moreover, the magnetic flux is quantized in a precisely same manner as for vortices, which is immediately seen after using (2.18) and $f(\infty) = 0$ in (2.5), flux is $F/(2\pi) = -N$. Notice also that the magnetic energy of oscillating solutions is always finite even for an infinite sample.

Oscillating solutions exist also for the type B conditions. However, the numerical analysis revealed that in this case the parameter a must vanish and hence the magnetic field is completely absent. Nevertheless, the scalar field configuration is nontrivial. In fact, one is left then with the nonlinear scalar field equation

$$\varphi'' + \frac{1}{r}\varphi' + \lambda(\varphi - \varphi^3) = 0, \quad (7.2)$$

which in the limit of $r \rightarrow \infty$, when φ approaches 0, reduces to the linearized equation (7.1).

It is evident, that it is enough to find explicitly only a solution $\varphi_1(r)$ for the case $\lambda = \kappa = 1$. For an arbitrary value of the coupling constant the solution is then given by $\varphi = \varphi_1(\sqrt{\lambda}r)$. In particular, this defines positions of extrema and zeros of $\varphi(r)$ for all values of λ from that of $\varphi_1(r)$. The latter evidently depends only on the value of the parameter b in (2.21). Numerical results are displayed in Figure 24.

As we already mentioned, for an infinite sample both energy and the Gibbs free energy are divergent for oscillating solutions. However, for a finite cylinder we discover convergent

results. As it is well known, the boundary conditions in the Ginzburg-Landau theory require vanishing of derivative $\varphi'|_{r=R} = 0$ on a cylinder's surface $r = R$. Using (7.2), one then finds from (2.16) that for such zero magnetic field oscillating solutions the Gibbs free energy is always negative,

$$\Delta\mathcal{G} = -\frac{\pi\mu^2}{2} \int_0^R dr r \varphi^4(r). \quad (7.3)$$

A curious conclusion is thus that for a finite sample in absence of an external magnetic field an oscillating state is energetically more preferable than a purely normal state.

We have calculated the Gibbs free energy for the oscillating solutions in finite samples. A boundary can be placed at any of the positions of extrema of the solutions, and the numerical results are displayed in Table XVI. We present explicitly only the case $\lambda = 1$, while for an arbitrary λ , the relevant data are easily obtained from Table XVI by replacing $(R, \Delta\mathcal{G})$ with $(R/\sqrt{\lambda}, \Delta\mathcal{G}/\lambda)$ (cf. (7.3)).

Oscillating scalar field solutions appear also if one takes instead of an electromagnetic theory a general relativistic gravitational theory [23]. The solutions for this Einstein-scalar-field theory describe a dark halo of galaxies or galaxy clusters, respectively. The oscillating behavior of the scalar field can be removed simply by adding a mass term for the scalar field potential. In this case one speaks about boson star solutions [24] which have some characteristics similar to the neutron stars but also decisive differences [25]. These boson stars could be formed in the very early universe from Higgs or axion particles. That stable configurations of these boson stars can exist was investigated with the help of the catastrophe theory [26].

8. DISCUSSION AND CONCLUSION

In each class of solutions the decisive role is played by the values of the parameters (a, b) which appear in the regularity conditions at the origin (2.18)-(2.19) and (2.20)-(2.21). All the solutions are obtained after a “fine tuning” of these parameters. It is worthwhile to

draw a kind of a “phase diagram” on the (a, b) plane which shows explicitly the domains of existence for different solutions. Since the vortices, flux tubes and the oscillating solutions all belong to the type A regularity conditions (2.18)-(2.19), we can display them on the same (a, b) -plane, see Figures 21 for different values of κ . The encircled dots denote the “position” of a vortex solution while each curve represents a complete family of a flux tube or oscillating solutions for a fixed κ . Notice that all curves end on the a -axis ($b = 0$) at the points which correspond to the half of the relevant limit magnetic field values, i.e., $a = \frac{1}{2}h_k, k = 0, 1, \dots$. Curves which represent flux tubes with increasing number of nodes are concentrating in the close neighborhood of the “oscillating” curve which seem to indicate that the oscillating solutions are unstable and a small perturbation may cause their decay into a nearby flux tube with a finite number of nodes. When moving along any flux tube curve away from the a -axis, one inevitably hits the vortex dot, where magnetization diverges.

Technically, it is impossible (because of the limitations on numerical precision) to make integration for the parameters (a, b) in the close vicinity of a vortex. Thus, from the data which we obtained, it is not clear what is the limiting value of an external magnetic field to which all the flux tube configurations approach when (a, b) are coming closer and closer to the vortex parameters (a^*, b^*) . We can see however (cf. Tables VII-XIV), that such a limit is close to the thermodynamic critical field h_c for each κ . The following simple argument demonstrates that in fact such a limit is equal to h_c . Let us formally compare the values of the Gibbs free energy for a vortex and for a flux tube solution. We find that these are equal when

$$\mathcal{E}_V - \mathcal{E}_{FT} = 2\pi H_{\text{ext}} \left(1 - \int_0^\infty dr r h_{\text{FT}} \right), \quad (8.1)$$

where the subscripts V and FT denote the vortex and flux tube variables, respectively. The right and the left hand sides are both formally divergent, but nevertheless one can use (8.1) and (2.6), and find [noticing that after a certain finite value of r one has $h_{\text{FT}} = h_{\text{ext}}$ and $\varphi_{\text{FT}} = 0$] $h_{\text{ext}} = (h_{\text{ext}}^2 + \frac{\lambda}{2}) / (2h_{\text{ext}})$, from which

$$h_{\text{ext}} = \sqrt{\frac{\lambda}{2}} = h_c. \quad (8.2)$$

Below (above) this value, the pure vortices (the flux tubes) are energetically more preferable.

Summarizing, in this paper we present the numerical solutions of the cylindrically symmetric Ginzburg-Landau equations. Besides the well known vortex configurations with finite energy we find new solutions (we call them type B and the flux tube solutions) which have finite Gibbs free energy. Direct numerical integration reveals many interesting properties of these solutions. One of the most important points is perhaps the clarification of the meaning and value of the upper critical field h_{c2} . Contrary to what is usually claimed in the literature, h_{c2} by no means denotes the magnetic field below which the vortex becomes more energetically preferable than the normal state. Instead, as we now understand, $h_{c2} = \lambda$ is the value of an external magnetic field at which the type B solutions and the flux tubes have zero Gibbs free energy. Below it, for $h_{\text{ext}} < h_{c2}$, $\Delta\mathcal{G}$ is negative for both flux tubes and type B configurations. The analysis of linearized Ginzburg-Landau equations near h_{c2} which usually (and incorrectly) is described in the literature (see, e.g., [3,5–9]) as relevant to vortices, in fact is the linearization of flux tubes and type B solutions. Our results show that the flux tube solutions without node remain the most energetically preferable from h_{c2} down to the thermodynamic critical field h_c , after which the vortices become energetically more preferable and such a vortex state ends at the lower critical field h_{c1} . We find it convenient to depict this observation on Figure 25. It is worthwhile to stress, that our results do not contradict the previous knowledge about the mixed state in the type II superconductors. On the contrary, they again support the significance of such a fundamental structure as a vortex: notice that, after all, one can interpret a flux tube solution as a vortex “surrounded” by a type B configuration. However, in our opinion, the flux tubes provide us with a new understanding that the mixed state reveals a rich structure in which a “pure vortex” is only part of the whole picture valid near h_{c1} . We are convinced that a correct transition from such a pure vortex state to the normal state (starting at h_c up to h_{c2}) can only be correctly described with the help of the flux tube and the type B solutions.

APPENDIX: CORRESPONDENCE WITH THE GINZBURG-LANDAU NOTATION

In the Ginzburg-Landau theory of superconductivity [1], the scalar field φ is interpreted as the “order parameter” with the square describing the “density of superconducting electrons”, $n_s = |\varphi|^2$. The potential is usually written in the form

$$\mathcal{V}_{GL} = \alpha|\varphi|^2 + \frac{\beta}{2}|\varphi|^4, \quad (\text{A.1})$$

with constant parameters $\alpha < 0, \beta > 0$. Their physical meaning is clarified by the following quantities they define: the thermodynamic critical magnetic field for a bulk superconductor $H_c^2 := \alpha^2/\beta$; the equilibrium density of superconducting electrons $|\varphi_\infty| := |\alpha|/\beta$; the order parameter coherence length $\xi := 1/\sqrt{2|\alpha|}$; the magnetic field penetration length $\delta := \sqrt{\beta/|\alpha|}$. (We are using the units in which the mass and the charge of the electron is equal one). Of particular importance is the ratio of two lengths

$$\kappa := \frac{\delta}{\xi}. \quad (\text{A.2})$$

Comparing (2.2) and (A.1), we find the relation between our and the Ginzburg-Landau notations:

$$\alpha = -\frac{\mu^2}{2}, \quad \beta = \frac{\lambda}{2}, \quad (\text{A.3})$$

hence, in our notation, we have

$$\xi = \frac{1}{\mu}, \quad \delta = \frac{\sqrt{\lambda}}{\mu}, \quad (\text{A.4})$$

$$\kappa = \sqrt{\lambda}, \quad 2H_c^2 = \frac{\mu^4}{\lambda}. \quad (\text{A.5})$$

Technically, there are also other notational differences: in the literature on type II superconductors instead of f one often uses $Q := -f/\sqrt{\lambda}$, while the dimensionless line energy density is defined [1,3,12,11,5–9] by

$$\epsilon := \frac{\mathcal{E}}{\delta^2 H_c^2} = \frac{2\pi}{\lambda} \left\{ [r\varphi'\varphi]_0^\infty + \int_0^\infty dr r \left[h^2 + \frac{\lambda}{2}(1 - \varphi^4) \right] \right\}, \quad (\text{A.6})$$

where we used the field equation (2.8).

Acknowledgments.

We would like to thank Friedrich W. Hehl and Eckehard W. Mielke for very useful criticism and advice. The work of YNO was supported by the Deutsche Forschungsgemeinschaft (Bonn) grant He 528/17-1, and for FES by the European Union.

REFERENCES

- [1] L.D. Landau and V.L. Ginzburg, *ZhETF* **20** (1950) 1064; English translation in: *Collected papers of L.D. Landau*, ed. D. Ter Haar (Pergamon Press: Oxford, 1965), 546-568.
- [2] H.B. Nielsen and P. Olesen, *Nucl. Phys.* **B61** (1973) 45-61.
- [3] A.A. Abrikosov, *Sov. Phys. JETP* **5** (1957) 1174-1182.
- [4] R. Owczarek, *Rept. Math. Phys.* **34** (1994) 305-310.
- [5] P.G. De Gennes, *Superconductivity of metals and alloys* (W.A. Benjamin: New York, 1966).
- [6] A.L. Fetter and P.C. Hohenberg, in: *Superconductivity* (Marcel Dekker: New York, 1969), Ed. R.D. Parks, p. 817-923.
- [7] D. Saint-James, E.J. Thomas, and G. Sarma, *Type II superconductivity* (Pergamon Press: Oxford, 1969).
- [8] R.P. Huebener, *Magnetic flux structures in superconductors* (Springer: Berlin, 1979).
- [9] V.V. Shmidt and G.S. Mkrtchyan, *Sov. Phys. Uspekhi* **17** (1974) 170-185.
- [10] L. Perivolaropoulos, *Phys. Rev.* **D48** (1993) 5961-5962.
- [11] J.L. Harden and V. Arp, *Cryogenics* **3** (1963) 105-108.
- [12] P. Tholfsen and H. Meissner, *Phys. Rev.* **169** (1968) 413-416.
- [13] H.J. Fink and A.G. Presson, *Phys. Rev.* **151** (1966) 219-228.
- [14] L. Neumann and L. Tewordt, *Z. Phys.* **189** (1966) 55-66.
- [15] R. Doll and P. Graf, *Z. Phys.* **197** (1966) 172-191.
- [16] L. Jacobs and C. Rebbi, *Phys. Rev.* **B19** (1979) 4486-4494.
- [17] P.S. Jang, S.Y. Park, and K.C. Wali, *Phys. Rev.* **D17** (1978) 1641-1650.

[18] F.A. Lunev, *Phys. Lett.* **B311** (1993) 273; D. Singleton, *Phys. Rev.* **D51** (1995) 5911; D. Singleton, *Axially symmetric solutions for $SU(2)$ Yang-Mills theory*, Preprint, *Lanl e-archive hep-th/9502116* (1995) 15 p.; Yu.N. Obukhov, *Confining string solutions of the Yang-Mills gauge theory*, Preprint Inst. for Theor. Phys., Univ. of Cologne (1995) 17 p.

[19] H.J. de Vega and F.A. Schaposnik, *Phys. Rev.* **D14** (1976) 1100-1106.

[20] E.J. Weinberg, *Phys. Rev.* **D19** (1979) 3008-3012.

[21] C.H. Taubes, *Commun. Math. Phys.* **72** (1980) 277-292.

[22] D.K. Finnemore, T.F. Stromberg, and C.A. Swenson, *Phys. Rev.* **149** (1966) 231-243.

[23] F. E. Schunck, *A matter model for dark halos of galaxies and quasars*, submitted to *Phys. Rev. Lett.* (1995).

[24] E. W. Mielke and R. Scherzer, *Phys. Rev.* **D24** (1981) 2111; P. Baekler, E. W. Mielke, R. Hecht, and F. W. Hehl, *Nucl. Phys.* **B288** (1987) 800; Ph. Jetzer, *Phys. Rep.* **220** (1992) 163; T. D. Lee and Y. Pang, *Phys. Rep.* **221** (1992) 251.

[25] F. E. Schunck, *Selbstgravitierende bosonische Materie*, Ph. D. thesis, Cologne (1995); F. E. Schunck and E. W. Mielke, *Radially rotating relativistic boson stars*, submitted to *Phys. Rev. Lett.* (1995); E.W. Mielke and F.E. Schunck, *Rotating boson stars*, in: “*Gravity, Particles and Space-Time*”, P. Pronin and G. Sardanashvily, eds. (World Scientific, Singapore 1996), p. 391-420; F.E. Schunck and E.W. Mielke, *Rotating boson stars*, *Proceedings of the Bad Honnef Workshop “Relativity and Scientific Computing: Computer Algebra, Numerics, Visualization”*, F.W. Hehl, R.A. Puntigam, and H. Ruder, eds. (Springer-Verlag, Berlin 1996), p. 8-11, 138-151.

[26] F. V. Kusmartsev, E. W. Mielke, and F. E. Schunck, *Phys. Rev.* **D43** (1991) 3895; *Phys. Lett.* **B157** (1991) 465.

FIGURES

FIG. 1. A typical vortex solution. At the center, the magnetic field h is maximal. The limit of the scalar field φ is 1, which means physically a completely superconducting state. With our gauge choice the potential is vanishing at infinity.

FIG. 2. The scalar field φ and the normalized magnetic field $h/(2a)$ for several values of κ . From these curves, one can read off the penetration lengths δ_{cal} of the scalar field and ξ_{cal} of the magnetic field which are determined at the $1/e$ level.

FIG. 3. The energy per unit length for vortices with flux $F/(2\pi) = -1$ ($N = 1$) and $F/(2\pi) = -2$ ($N = 2$). For comparison, the double energy value of the 1-vortex is also given. One recognizes clearly that for $\kappa > 1/\sqrt{2}$ (the vertical line) a 1-vortex is energetically more preferable than a 2-vortex.

FIG. 4. The comparison of the formal parameter κ , which appears in the Ginzburg-Landau system, and of the ratio δ_{cal}/ξ_{cal} calculated from the solution of the Ginzburg-Landau system. Near $\kappa = 1.0$, we find an essential deviation for $F/(2\pi) = -1, -2$.

FIG. 5. Type B solutions without node for $\kappa = 1.0$: The scalar field φ with initial values $\varphi(0) = 0.9, 0.6, 0.3$ and $f(0) = 0.0$.

FIG. 6. The same type B solutions without node for $\kappa = 1.0$ as in Fig. 5: The potential f and the magnetic field h .

FIG. 7. Type B solutions without node with very high magnetization. The scalar field φ has initial values which are almost 1 (see Table IV). With increasing magnetization the scalar field has a wider central core where it is almost 1, i.e. full superconductivity at the center. When the scalar field becomes zero, the magnetic field achieves a constant value.

FIG. 8. Type B solutions with one node for $\kappa = 1.0$: The scalar field φ with initial values $\varphi(0) = 0.9, 0.6, 0.3$ and $f(0) = 0.0$.

FIG. 9. The same type B solutions with one node for $\kappa = 1.0$ as in Fig. 8: The potential f and the magnetic field h . At zeros of the scalar field, the magnetic field has a step-like behavior. For the constant magnetic field, the potential grows as r^2 .

FIG. 10. Flux tube solutions without node: The scalar field φ for $\kappa = 0.5, 1.0, 1.5$ with the same magnetization $M/(2\pi) = 6.0$. The scalar field of a flux tube produces a maximum before going to zero (and not to 1, as in the case of vortices).

FIG. 11. Flux tube solutions without node: The potential f and the magnetic field h for $\kappa = 0.5, 1.0, 1.5$ with the same magnetization $M/(2\pi) = 6.0$. The potential starts at 1, is followed by a minimum and then grows with an asymptotic r^2 behavior, so that the magnetic field is constant.

FIG. 12. Flux tube solutions without node: Configurations with external magnetic field near h_c . Both solutions are close to the vortex solution for $\kappa = 1.0$ which ‘lies’ between these two flux tube solutions; cf. Table VIII. The dotted curve has a negative Gibbs free energy, while the drawn curve has positive Gibbs free energy. Coming closer and closer to the vortex, the magnetization increases without a limit, while the scalar field at the center approaches the vortex configuration, and simultaneously the interval grows where it is almost 1. Such a limit flux tube consists then of a vortex in the center and a type B solution at higher radial values. The initial values (a, b) of this solution are close to that of the vortex; cf. Table I.

FIG. 13. The same flux tube solutions without node as in Fig. 12: potential and magnetic field configurations.

FIG. 14. Flux tube solutions with one node: A solution near h_c with negative Gibbs free energy. The scalar field has one node while the magnetic field has a ‘step’ at the node’s position. Again one can describe this solution as a combination of a vortex at the center and a type B solution outwards.

FIG. 15. Magnetization curves for type B solutions without (right curve) and with one node (left curve) for different κ . For $\kappa = 2.25$, we notice a change of the sign of the Gibbs free energy within a solution family. For $\kappa = 0.5, 1.0, 1.5$ we find only positive values of \mathcal{G} .

FIG. 16. The magnetization curve for flux tube solutions with $\kappa = 0.5, 1.0, 1.5$ for a scalar field without node. For each κ , the corresponding limit values h_1 , h_2 , h_c , and h_{c2} is drawn. For instance, the curve for $\kappa = 1.0$ has a branch with a negative Gibbs free energy in the range $[h_c, h_{c2}] = [0.707, 1.0]$ of the external magnetic field and a branch with positive values in the range of $[h_1, h_c] = [1/3, 0.707]$. The magnetization diverges at h_c . For $\kappa = 0.5$ the point h_c does not lie within the two limits h_1 and h_{c2} so that one can find also solutions up to h_c . The lower figure displays in detail how the branches of solutions with positive and negative $\Delta\mathcal{G}$ behave near the h_c limit ($\kappa = 1$).

FIG. 17. Magnetization curve for flux tube solutions with $\kappa = 1.0$ for a scalar field without (limits $[h_1, h_{c2}]$) and with one node (limits $[h_2, h_1]$). In both cases the magnetization diverges at the external magnetic field h_c which is the limiting point for the vortex.

FIG. 18. $\Delta\mathcal{G}$ against the external magnetic field for $\kappa = 1.0$ for the flux tube and the type B solutions.

FIG. 19. $\Delta\mathcal{G}$ against the external magnetic field for $\kappa = 2.25$ for the flux tubes and the type B solutions. The lower figure gives an enlarged view of the flux tube curve with one node, while the broken line denotes type B solutions with one node. In each case the flux tubes have lower values of $\Delta\mathcal{G}$ than the type B solutions. Hence, flux tubes are energetically more preferable.

FIG. 20. $\Delta\mathcal{G}$ against the external magnetic field for $\kappa = 5.0$ flux tubes without and with one node. Both curves limits into h_c .

FIG. 21. (a, b) diagrams for $\kappa = 1.0, 2.25, 5.0$. The big dot describes in each case the corresponding vortex solution. The drawn, broken and dotted lines represent the flux tubes without node, the flux tubes with one node, and the oscillating solutions, respectively. The type B solutions cannot be compared in these diagrams because they have different initial values.

FIG. 22. The oscillating solutions for type A initial conditions. For an initial value (here, $b = 0.777$) very near to the one of the vortex, the scalar field has a part which is almost 1 before the oscillation starts. At the center, the vortex can be recognized. No oscillating solution with an initial value above that of the vortex can be found.

FIG. 23. This figure shows what happens with the magnetic field for an oscillating scalar field. At the zeros of the scalar field, the magnetic field has a step-like behavior. As in the case of the vortex, the magnetic field quickly vanishes, and the flux of the oscillating solution is quantized. Here, we have $F/(2\pi) = -1$.

FIG. 24. The oscillating solution for type B. Here, a solution with a non-vanishing magnetic field does not exist. The square of the scalar field, the density of superconducting electrons, oscillates without any external magnetic field, and every finite sample has a negative Gibbs free energy.

FIG. 25. The general diagram for different solutions. The vortex state is energetically most preferable between H_{c1} and H_c , while above H_c , the flux tube configurations replace them. Hence, H_c gains the following physical meaning for a type II superconductor: Above H_c , isolated vortices come into contact with the external magnetic field and the flux tube solutions are constructed. Energetically, the most preferable solution is a flux tube without node. But also the flux tubes with nodes do exist there, if κ is large enough. Near H_{c2} , only the flux tube without node exists. Of course, the flux tubes ‘live’ also in the vortex and the Meissner state but they are energetically less preferable. In this way, we find a rich fine structure of a superconductor’s mixed state.

Figure 1:

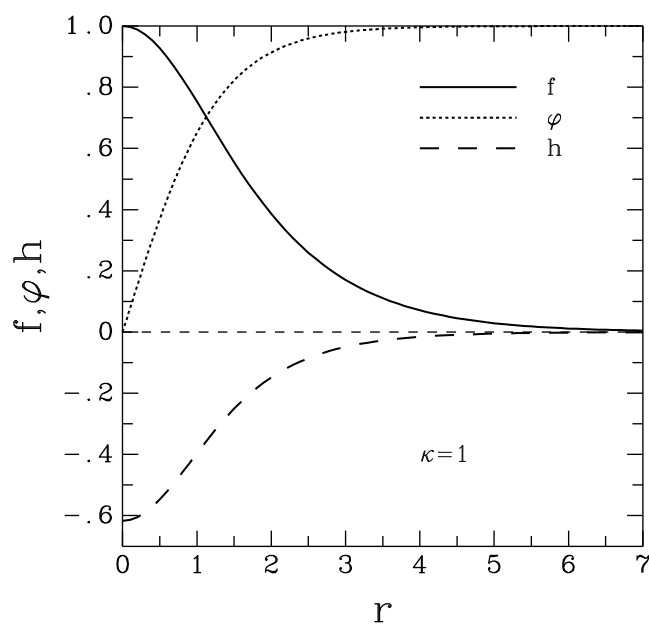


Figure 2:

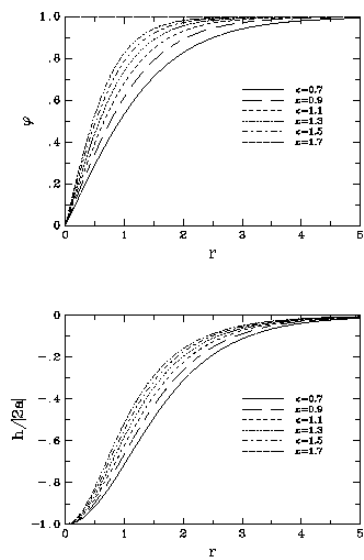


Figure 3:

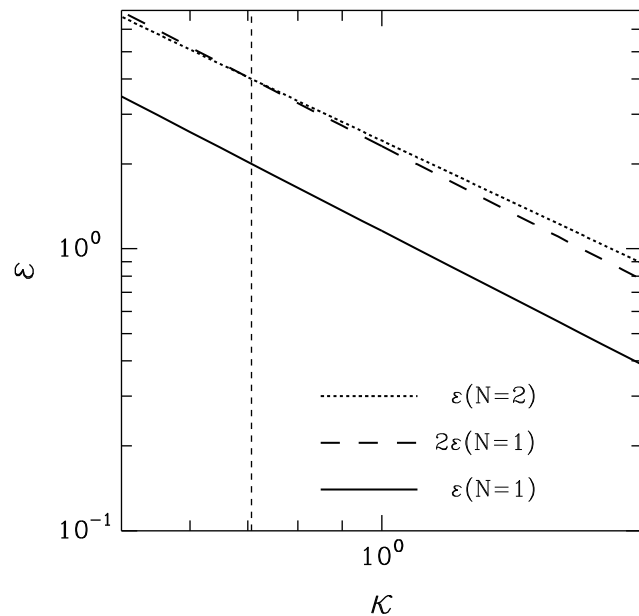


Figure 4:

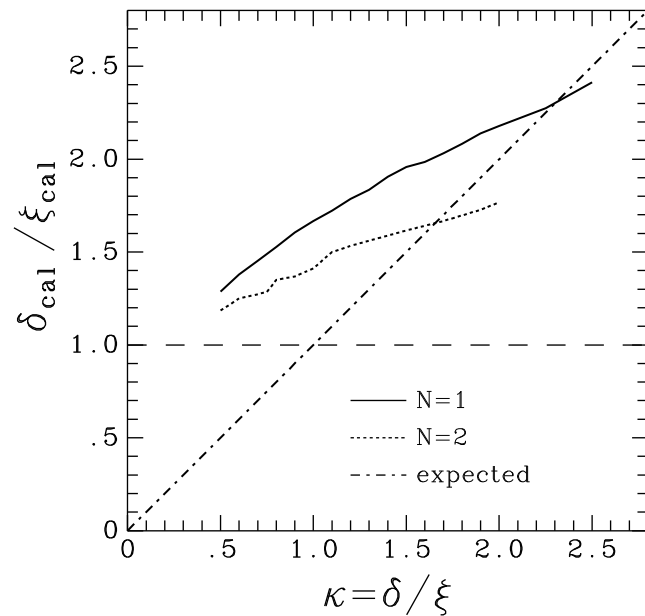


Figure 5:

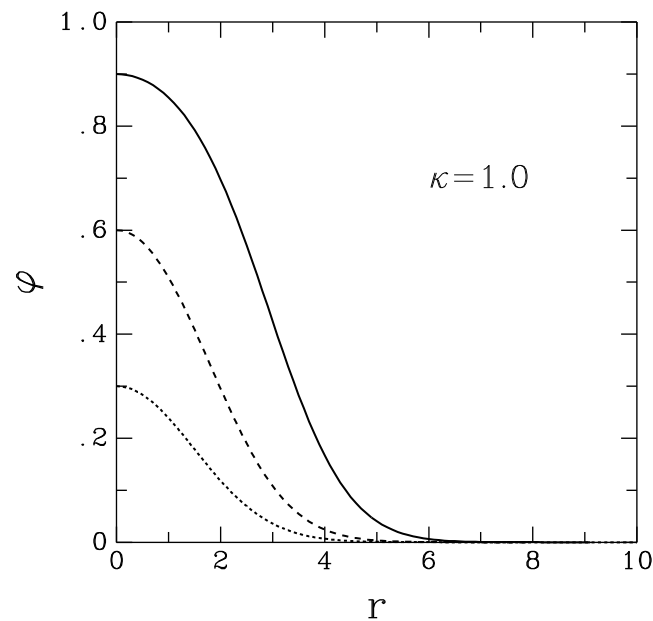


Figure 6:

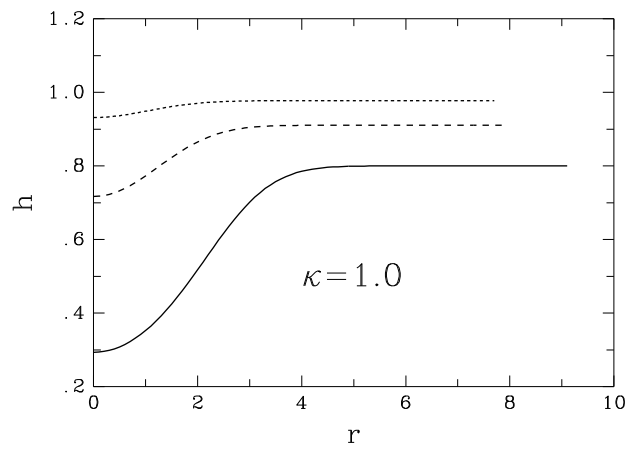
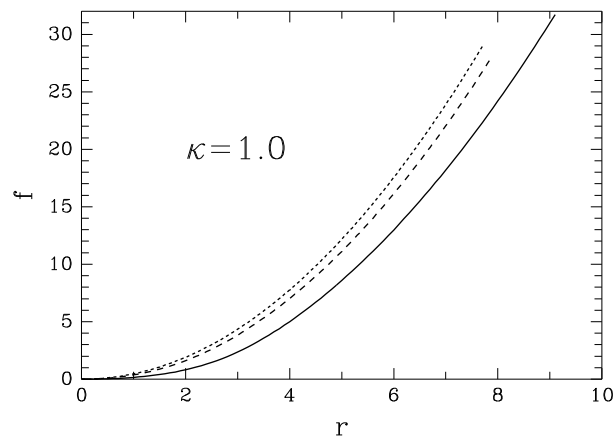


Figure 7:

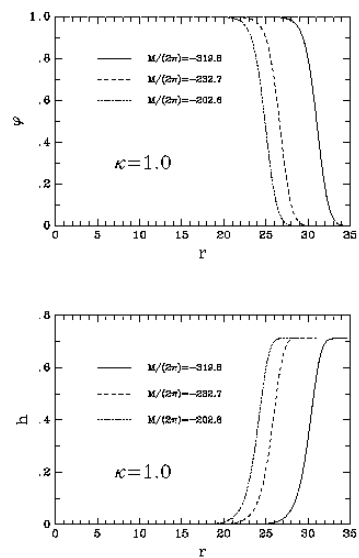


Figure 8:

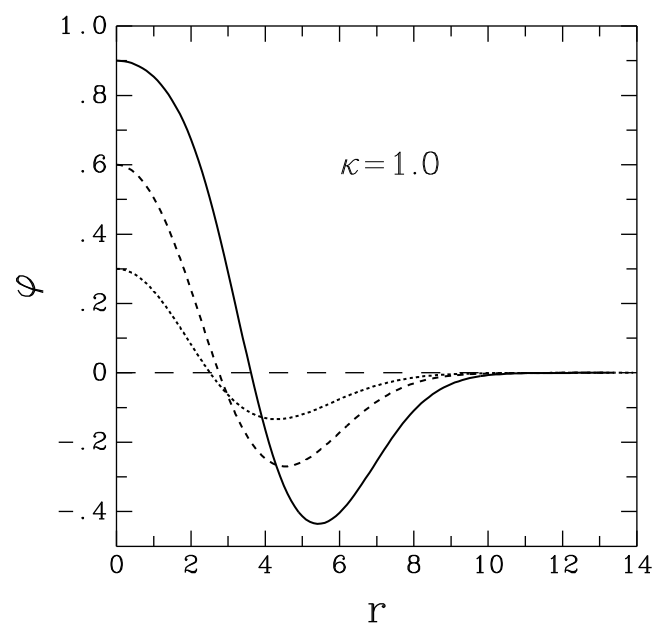


Figure 9:

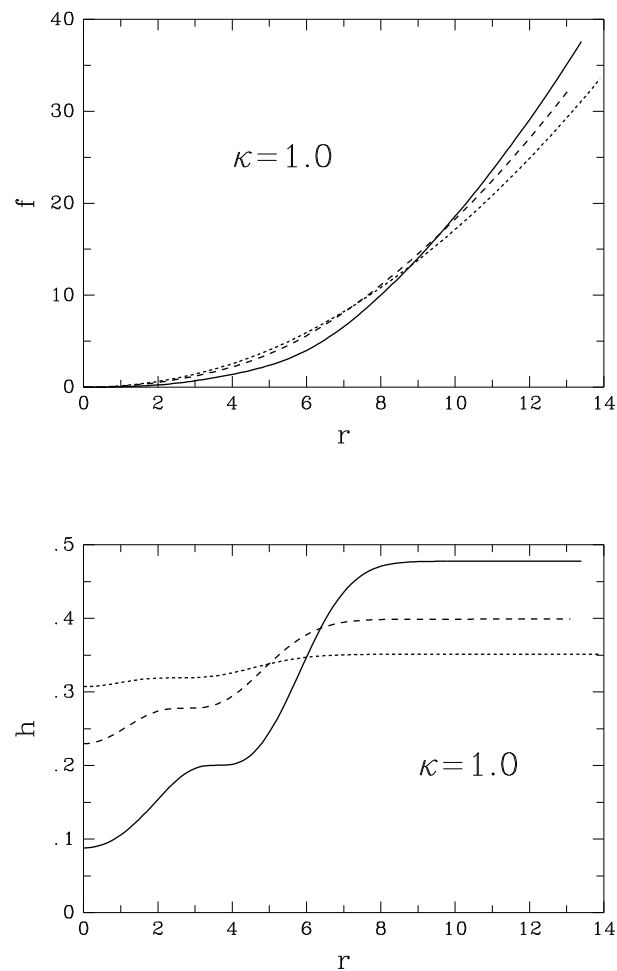


Figure 10:

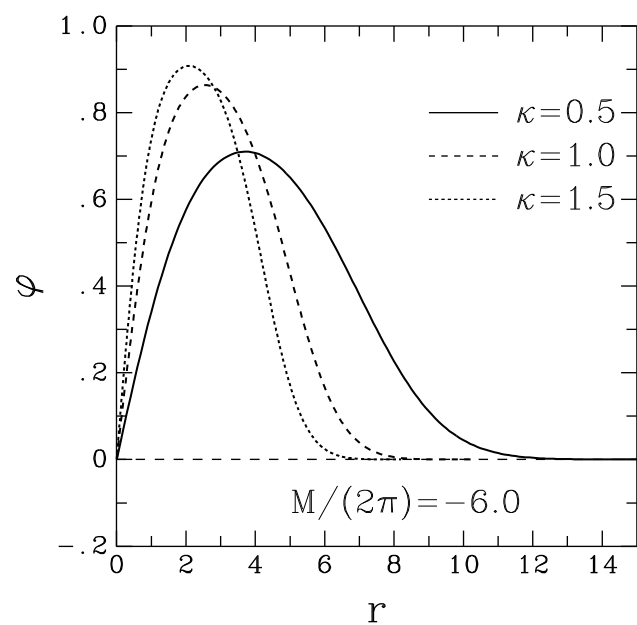


Figure 11:

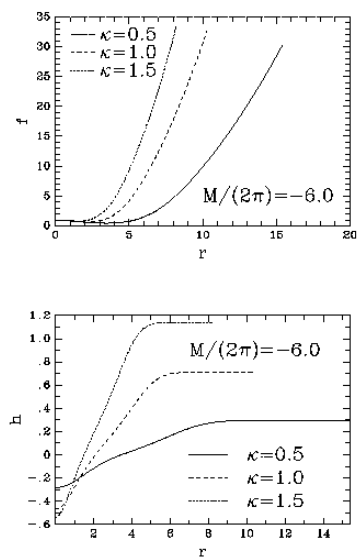


Figure 12:

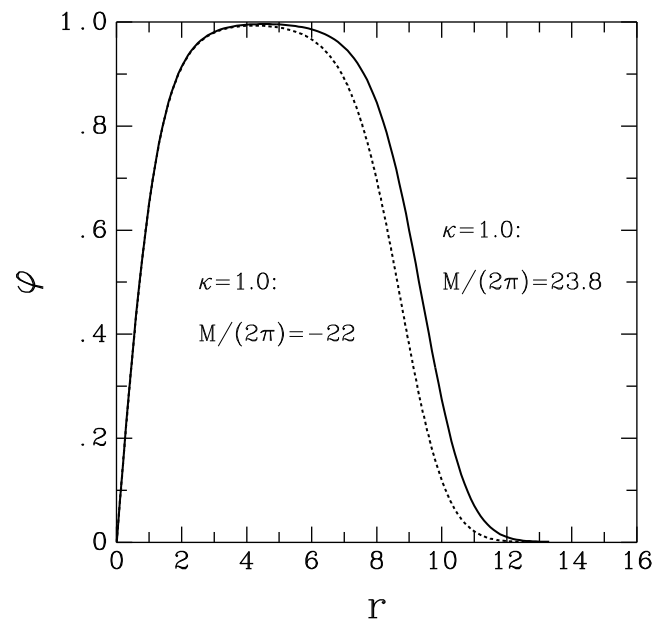


Figure 13:

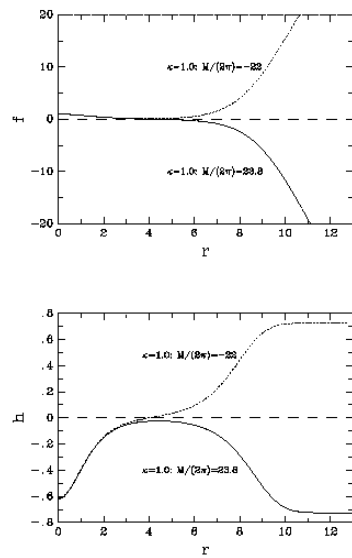


Figure 14:

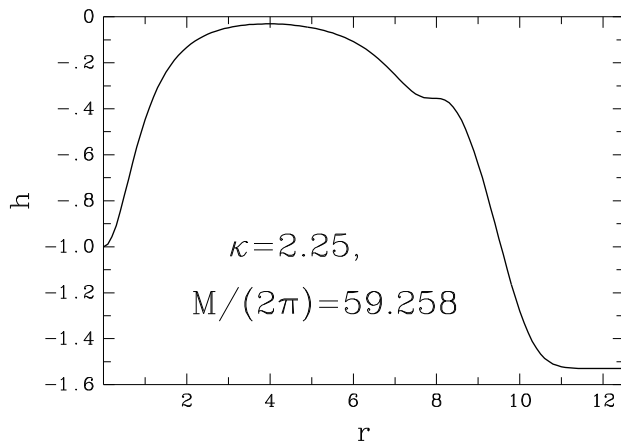
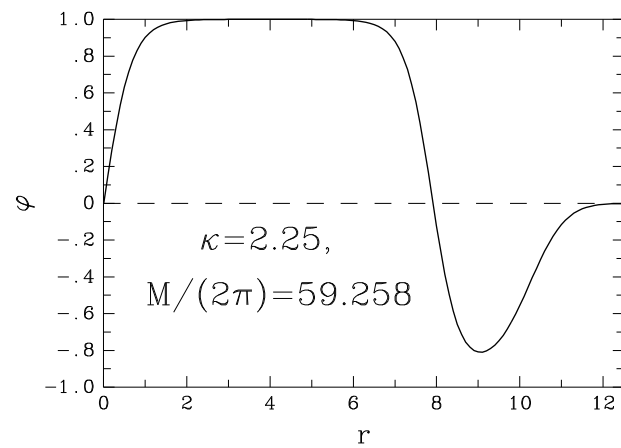


Figure 15:

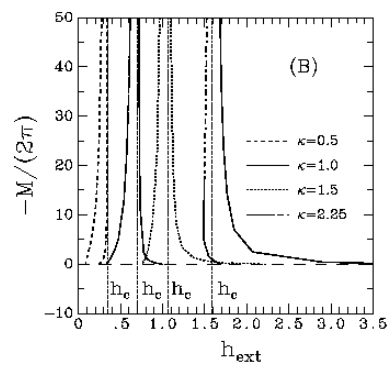


Figure 16:

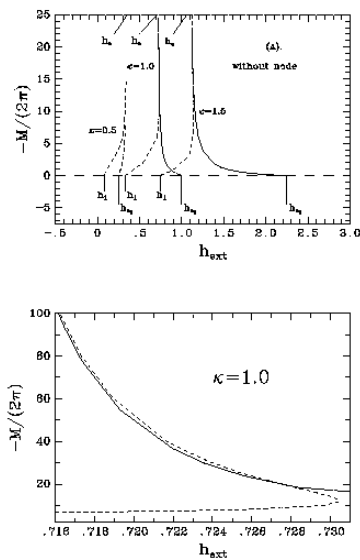


Figure 17:

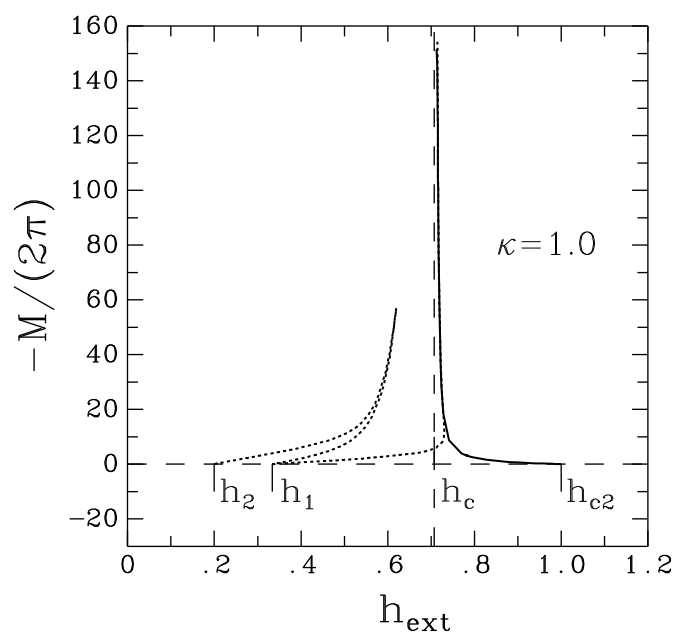


Figure 18:

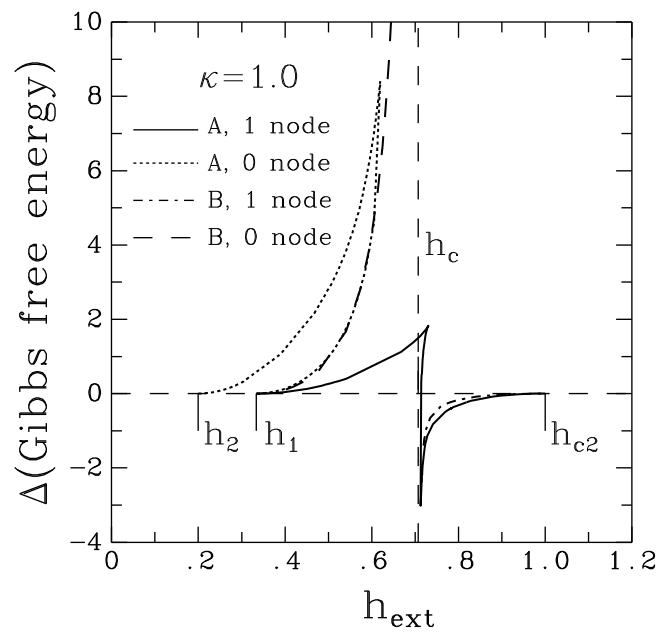


Figure 19:

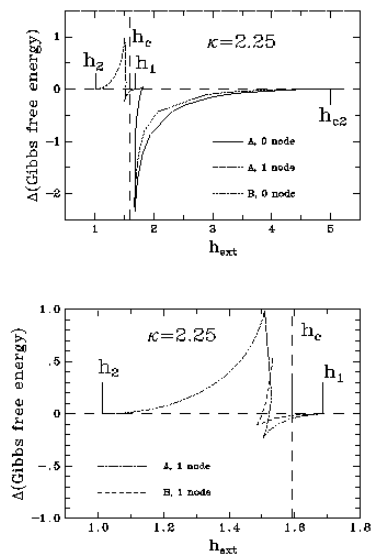


Figure 20:

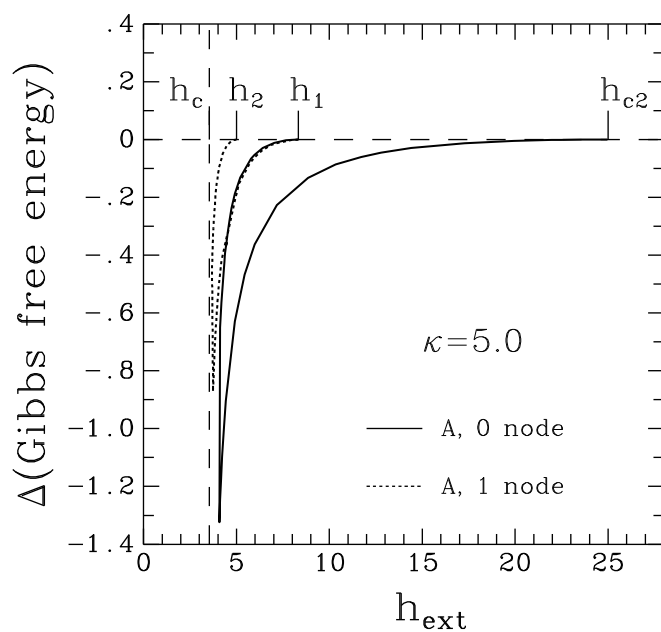


Figure 21:

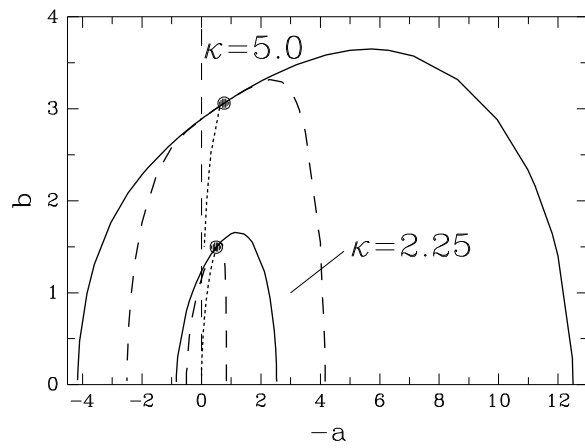
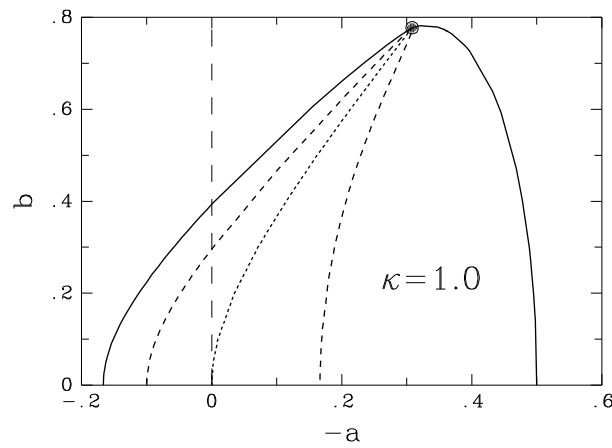


Figure 22:

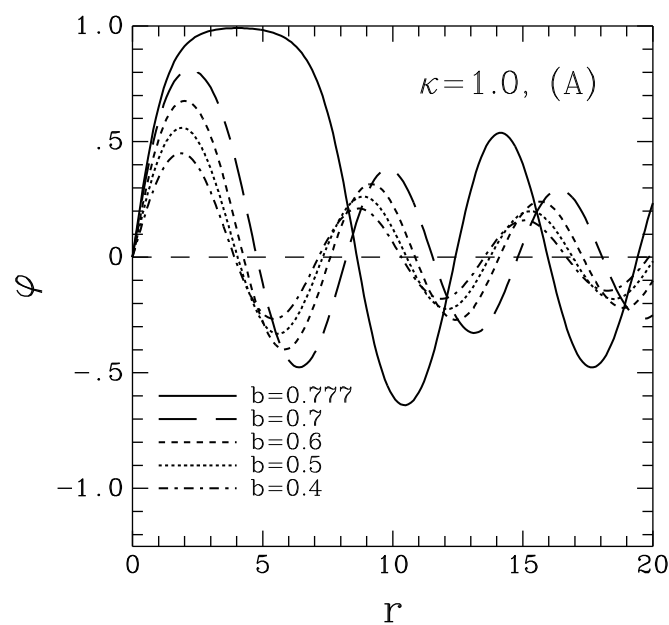


Figure 23:

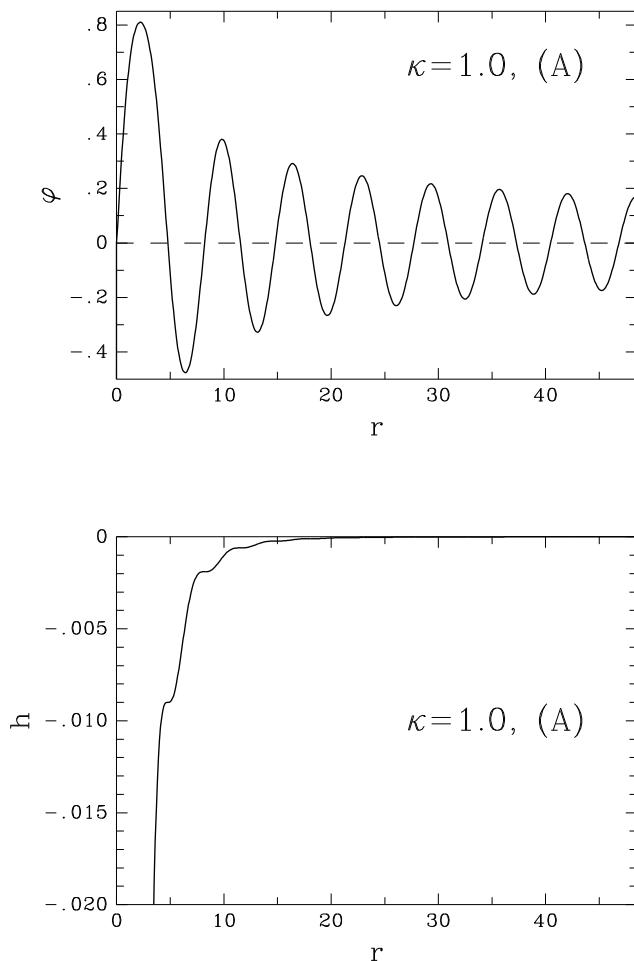


Figure 24:

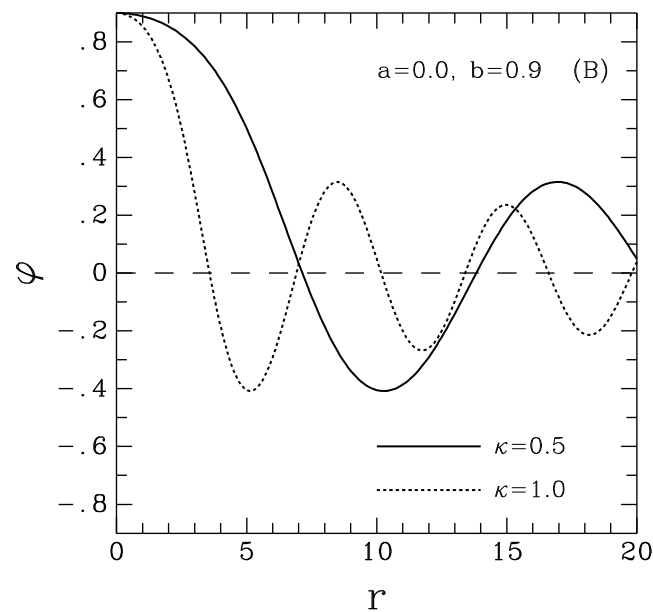
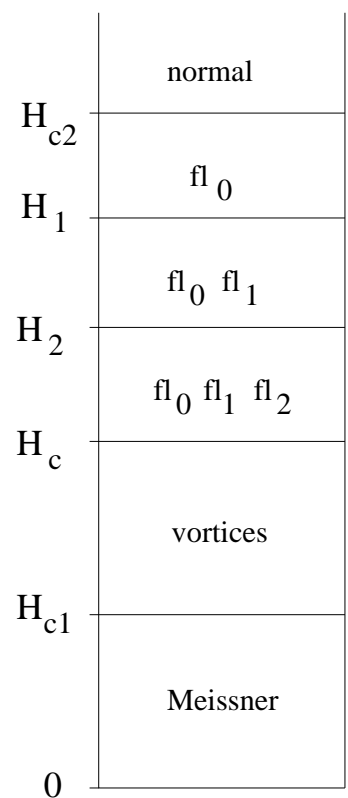


Figure 25:



TABLES

TABLE I. Vortex solutions

κ	$N = 1$				$N = 2$			
	a	b	$\mathcal{E}[\pi\mu^2]$	$\frac{H_{c1}}{\sqrt{2}H_c}$	a	b	$\mathcal{E}[\pi\mu^2]$	$\frac{H_{c1}}{\sqrt{2}H_c}$
2.00	-0.46614	1.35218	0.38816	0.38816	-0.52764	1.01524	0.88928	0.44464
1.75	-0.43108	1.20961	0.47922	0.41932	-0.48000	0.82862	1.07872	0.47194
1.50	-0.39344	1.06659	0.61094	0.45821	-0.42993	0.65857	1.34754	0.50532
1.25	-0.35273	0.92273	0.81402	0.50876	-0.37708	0.50680	1.75284	0.54776
1.00	-0.30828	0.77735	1.15676	0.57838	-0.32096	0.37219	2.41915	0.60478
0.75	-0.25904	0.62916	1.82190	0.68321	-0.26080	0.25461	3.67126	0.68836
$1/\sqrt{2}$	-0.25000	0.60328	1.99999	0.70710	-0.25000	0.23614	3.99999	0.70710
0.50	-0.20314	0.47525	3.47164	0.86791	-0.19527	0.15401	6.64856	0.83107

 TABLE II. Type B solutions for $\kappa = \sqrt{1/2}$.

b	a	$F/(2\pi)$	$\Delta\mathcal{G} [\pi\mu^2]$	h_{ext}
$1 - 10^{-16}$	$0.81463 \cdot 10^{-19}$	-506.26448	0.0	0.5
$1 - 10^{-8}$	$0.50000 \cdot 10^{-8}$	-97.79618	0.0	0.5
$1 - 10^{-4}$	$0.49997 \cdot 10^{-4}$	-26.47560	0.0	0.5
0.9	0.04750	-2.24829	0.0	0.5
0.7	0.12750	-0.76485	0.0	0.5
0.5	0.18750	-0.30398	0.0	0.5
0.3	0.22750	-0.09603	0.0	0.5
0.1	0.24750	-0.01006	0.0	0.5
0.0	0.25000	0.00000	0.0	0.5

TABLE III. Type B solutions for $\kappa = 0.5$.

b	Without node				With one node			
	a	$M/(2\pi)$	$\Delta\mathcal{G} [\pi\mu^2]$	h_{ext}	a	$M/(2\pi)$	$\Delta\mathcal{G} [\pi\mu^2]$	h_{ext}
$1 - 10^{-12}$	$2.27 \cdot 10^{-18}$	-303.481	7.062	0.350	$2.07 \cdot 10^{-20}$	-407.838	76.685	0.324
$1 - 10^{-8}$	$1.11 \cdot 10^{-12}$	-140.171	4.908	0.349	$1.69 \cdot 10^{-14}$	-207.472	50.180	0.312
$1 - 10^{-4}$	$5.73 \cdot 10^{-7}$	-38.359	2.523	0.345	$1.98 \cdot 10^{-8}$	-70.925	23.942	0.285
0.9	0.0111	-3.500	0.621	0.323	0.0014	-12.103	4.794	0.207
0.7	0.0464	-1.298	0.212	0.299	0.0092	-6.058	1.827	0.164
0.5	0.0816	-0.555	0.057	0.277	0.0207	-3.262	0.618	0.131
0.3	0.1085	-0.185	0.007	0.260	0.0326	-1.360	0.112	0.104
0.1	0.1231	-0.020	0.000	0.251	0.0405	-0.175	0.001	0.085
0.0	0.1250	0.000	0.000	0.250	0.0414	0.000	0.000	0.083

TABLE IV. Type B solutions for $\kappa = 1.0$.

b	Without node				With one node			
	a	$M/(2\pi)$	$\Delta\mathcal{G} [\pi\mu^2]$	h_{ext}	a	$M/(2\pi)$	$\Delta\mathcal{G} [\pi\mu^2]$	h_{ext}
$1 - 10^{-16}$	$2.62 \cdot 10^{-13}$	-319.831	-3.336	0.712	$1.88 \cdot 10^{-14}$	-399.137	22.180	0.672
$1 - 10^{-12}$	$2.80 \cdot 10^{-9}$	-150.422	-2.301	0.714	$2.62 \cdot 10^{-10}$	-201.853	14.548	0.659
$1 - 10^{-8}$	$1.79 \cdot 10^{-6}$	-69.240	-1.582	0.718	$2.20 \cdot 10^{-7}$	-102.176	9.272	0.641
$1 - 10^{-4}$	$1.11 \cdot 10^{-3}$	-18.774	-0.846	0.728	$2.11 \cdot 10^{-4}$	-34.388	4.108	0.597
0.9	0.1466	-1.412	-0.169	0.800	0.0439	-5.299	0.610	0.477
0.7	0.3030	-0.430	-0.042	0.878	0.0957	-2.376	0.188	0.420
0.5	0.4033	-0.160	-0.009	0.937	0.1307	-1.126	0.051	0.380
0.3	0.4659	-0.048	-0.001	0.977	0.1536	-0.401	0.007	0.351
0.1	0.4962	-0.005	$-1.25 \cdot 10^{-5}$	0.997	0.1652	-0.044	$9.30 \cdot 10^{-5}$	0.335
0.0	0.5000	0.000	0.000	1.000	0.1666	0.000	0.000	0.333

TABLE V. Type B solutions for $\kappa = 1.5$.

b	Without node				With one node			
	a	$M/(2\pi)$	$\Delta\mathcal{G} [\pi\mu^2]$	h_{ext}	a	$M/(2\pi)$	$\Delta\mathcal{G} [\pi\mu^2]$	h_{ext}
$1 - 10^{-12}$	$9.05 \cdot 10^{-7}$	-120.085	-2.907	1.086	$5.28 \cdot 10^{-7}$	-137.936	4.587	1.005
$1 - 10^{-8}$	$9.49 \cdot 10^{-5}$	-55.452	-2.020	1.098	$4.87 \cdot 10^{-5}$	-69.413	2.759	0.984
$1 - 10^{-4}$	0.0107	-14.519	-1.078	1.136	$4.85 \cdot 10^{-3}$	-22.896	1.033	0.936
$1 - 10^{-2}$	0.1248	-3.503	-0.513	1.228	0.0518	-8.131	0.313	0.878
0.9	0.4321	-0.780	-0.159	1.470	0.1638	-3.078	0.085	0.830
0.7	0.7550	-0.208	-0.033	1.802	0.2666	-1.256	0.023	0.796
0.5	0.9460	-0.073	-0.006	2.027	0.3232	-0.552	0.005	0.774
0.3	1.0623	-0.021	$-7.51 \cdot 10^{-4}$	2.170	0.3569	-0.185	$7.44 \cdot 10^{-4}$	0.759
0.1	1.1181	-0.002	$-8.71 \cdot 10^{-6}$	2.241	0.3730	-0.020	$9.25 \cdot 10^{-6}$	0.751
0.0	1.1250	0.000	0.000	2.250	0.3750	0.000	0.000	0.750

TABLE VI. Type B solutions for $\kappa = 2.25$.

b	Without node				With one node			
	a	$M/(2\pi)$	$\Delta\mathcal{G} [\pi\mu^2]$	h_{ext}	a	$M/(2\pi)$	$\Delta\mathcal{G} [\pi\mu^2]$	h_{ext}
$1 - 10^{-8}$	$3.96 \cdot 10^{-4}$	-66.111	-2.249	1.670	$3.96 \cdot 10^{-4}$	-70.821	0.526	1.534
$1 - 10^{-4}$	0.0396	-14.189	-1.107	1.765	0.0337	-17.351	$-4.34 \cdot 10^{-2}$	1.495
$1 - 10^{-2}$	0.3836	-2.443	-0.428	2.069	0.2154	-5.055	-0.101	1.486
0.9	1.1088	-0.402	$-9.99 \cdot 10^{-2}$	2.892	0.4756	-1.673	$-3.78 \cdot 10^{-2}$	1.544
0.7	1.7810	$-9.67 \cdot 10^{-2}$	$-1.83 \cdot 10^{-2}$	3.865	0.6640	-0.621	$-8.38 \cdot 10^{-3}$	1.613
0.5	2.1691	$-3.33 \cdot 10^{-2}$	$-3.52 \cdot 10^{-3}$	4.475	0.7597	-0.259	$-1.72 \cdot 10^{-3}$	1.652
0.3	2.4044	$-9.81 \cdot 10^{-3}$	$-3.90 \cdot 10^{-4}$	4.855	0.8147	$-8.41 \cdot 10^{-2}$	$-1.97 \cdot 10^{-4}$	1.675
0.1	2.5173	$-9.98 \cdot 10^{-4}$	$-4.48 \cdot 10^{-6}$	5.039	0.8405	$-8.93 \cdot 10^{-3}$	$-2.30 \cdot 10^{-6}$	1.686
0.0	2.53125	0.000	0.000	5.0625	0.84375	0.000	0.000	1.6875

TABLE VII. Flux-tube solutions for $\kappa = 0.50$

a	b	$M/(2\pi)$	$\Delta\mathcal{G} [\pi\mu^2]$	h_{ext}
0.04153	0.00482	-0.01000	0.00001	0.08362
0.03187	0.04510	-0.59999	0.04786	0.10262
0.00943	0.09464	-1.49999	0.35425	0.13855
-0.00711	0.12627	-2.00000	0.67207	0.16122
-0.06611	0.23111	-3.50000	2.14659	0.22868
-0.14000	0.35942	-5.89146	4.56113	0.29539
-0.19000	0.44962	-11.08773	6.82325	0.33221
0.20029	0.46875	-14.60379	2.20390	0.33977
0.16000	0.34108	-2.52520	0.43874	0.30136
0.12500	0.00100	-0.00001	$3.19979 \cdot 10^{-11}$	0.25000

TABLE VIII. Flux-tube solutions for $\kappa = 1.00$

a	b	$M/(2\pi)$	$\Delta\mathcal{G} [\pi\mu^2]$	h_{ext}
0.16666	0.00192	-0.00010	$1.01853 \cdot 10^{-9}$	0.33334
0.09149	0.24083	-0.99999	0.10874	0.44085
0.00770	0.38158	-1.90000	0.37497	0.53338
-0.00172	0.39592	-2.00000	0.41094	0.54261
-0.29562	0.76607	-12.00000	1.82881	0.73048
-0.30818	0.77728	-40.00000	1.39704	0.72168
-0.30828	0.77735	-154.22042	0.28830	0.71452
0.30828	0.77735	-151.56514	-3.02337	0.71300
0.39637	0.72724	-1.59999	-0.20076	0.82705
0.49998	0.00999	-0.00010	$-0.02499 \cdot 10^{-7}$	0.99997

TABLE IX. Flux-tube solutions for $\kappa = 1.50$

a	b	$M/(2\pi)$	$\Delta\mathcal{G} [\pi\mu^2]$	h_{ext}
0.37338	0.04336	-0.01000	0.00786 10^{-3}	0.75176
0.29017	0.32503	-0.50000	0.01852	0.83476
0.20216	0.47718	-1.00000	0.06744	0.90884
-0.08153	0.81864	-2.99999	0.34444	1.07986
-0.32032	1.02063	-8.09999	0.58261	1.14350
-0.38396	1.06126	-19.00079	0.36778	1.12618
-0.39033	1.06487	-26.99363	0.16315	1.11607
0.39368	1.06672	-43.31969	-5.99946	1.00392
0.60827	1.12205	-2.00000	-0.42922	1.36989
1.12490	0.02249	-0.00010	-0.00001 10^{-3}	2.24980

TABLE X. Flux-tube solutions for $\kappa = 2.25$

a	b	$M/(2\pi)$	$\Delta\mathcal{G} [\pi\mu^2]$	h_{ext}
0.84325	0.03080	-0.00100	0.26603 10^{-7}	1.68763
0.43741	0.87389	-1.00000	0.01468	1.77541
0.00000	1.23234	-3.01667	0.04214	1.81791
-0.01143	1.23977	-3.10000	0.04244	1.81815
-0.33764	1.42257	-8.00000	-0.01708	1.79367
-0.49780	1.49403	-55.15382	-1.03703	1.68033
0.50045	1.49512	-49.99032	-2.32259	1.68233
0.70035	1.56827	-5.00000	-0.85686	1.94614
1.13578	1.65419	-1.20000	-0.30921	2.52009
2.53100	0.03330	-0.00004	-4.27708 10^{-9}	5.06200

TABLE XI. Flux-tube solutions for $\kappa = 5.00$

a	b	$M/(2\pi)$	$\Delta\mathcal{G} [\pi\mu^2]$	h_{ext}
4.16596	0.04810	-0.00010	-3.42674 10^{-9}	8.33247
2.46720	2.08399	-0.50000	-0.02888	6.41076
0.00000	2.88809	-7.25261	-0.36536	4.43486
-0.06903	2.90474	-8.00000	-0.39067	4.39333
-0.21388	2.93905	-9.99944	-0.45318	4.30597
-0.50000	3.00438	-17.68306	-0.64910	4.12187
0.90370	3.09142	-25.02259	-1.32404	4.07299
1.65490	3.23837	-5.00000	-0.62843	4.91311
5.00000	3.63660	-0.29690	-0.08628	10.34339
12.48466	0.25004	-0.00010	-1.22344 10^{-7}	24.96932

TABLE XII. Flux-tube solutions with one node for $\kappa = 1.00$

a	b	$M/(2\pi)$	$\Delta\mathcal{G} [\pi\mu^2]$	h_{ext}
0.09500	0.05752	-0.19829	0.00122	0.20615
0.05000	0.19570	-1.69647	0.09688	0.25596
0.00000	0.29595	-3.05989	0.32649	0.30418
-0.10000	0.46591	-5.59633	1.05752	0.38929
-0.28500	0.74590	-15.43754	3.86498	0.54164
-0.30825	0.77732	-56.97949	8.41376	0.61958
0.30840	0.77735	-39.22317	4.61063	0.60533
0.30000	0.74194	-10.80591	1.55832	0.53261
0.18000	0.23311	-0.71579	0.01761	0.35821
0.16670	0.01173	-0.00185	0.00012 10^{-3}	0.33339

TABLE XIII. Flux-tube solutions with one node for $\kappa = 2.25$

a	b	$M/(2\pi)$	$\Delta\mathcal{G} [\pi\mu^2]$	h_{ext}
0.50620	0.01167	-0.00033	0.22768 10^{-8}	1.01253
0.50000	0.13056	-0.04152	0.00003	1.01681
0.00000	1.15113	-3.75047	0.18242	1.29551
-0.10000	1.24623	-4.83323	0.25732	1.33996
-0.45000	1.47366	-17.70122	0.75503	1.48389
-0.48750	1.48977	-30.99115	0.98537	1.50896
0.50000	1.49494	-59.25824	0.14568	1.53019
0.55000	1.51459	-14.74916	-0.22530	1.50431
0.70000	1.52843	-4.58431	-0.09886	1.54911
0.84373	0.03177	-0.00053	0.00000	1.68747

TABLE XIV. Flux-tube solutions with one node for $\kappa = 5.00$

a	b	$M/(2\pi)$	$\Delta\mathcal{G} [\pi\mu^2]$	h_{ext}
4.16660	0.03194	-0.00002	-1.17604 10^{-10}	8.33320
2.30000	3.31897	-1.97604	-0.15417	5.11558
0.90000	3.09064	-26.43953	-0.87154	3.73762
-0.69000	3.04608	-37.39455	-0.44849	3.68172
-0.60000	3.02649	-25.05396	-0.36250	3.71708
-0.50000	3.00438	-18.71862	-0.30676	3.74928
0.00000	2.88783	-7.65473	-0.16951	3.89400
1.00000	2.57972	-2.15981	-0.04797	4.26240
2.35000	1.02401	-0.11597	-0.00036	4.92020
2.49975	0.04278	-0.00018	-9.81200 10^{-10}	4.99986

TABLE XV. Type A oscillating solutions for $\kappa = 1.0$ and flux $F/(2\pi) = -1$.

a	b	$\mathcal{E}_{\text{mag}} [\pi\mu^2]$
-0.30828	0.77735	0.24523
-0.30809	0.77700	0.24493
-0.30700	0.77500	0.24328
-0.26629	0.70000	0.18786
-0.21314	0.60000	0.12758
-0.16217	0.50000	0.08008
-0.11438	0.40000	0.04429
-0.07120	0.30000	0.01975
-0.03500	0.20000	0.00579
-0.00955	0.10000	0.00058
-0.00246	0.05000	0.00005

TABLE XVI. Type B oscillating solutions for $\kappa = 1.0$. R gives the positions of extrema.

	R (minima)	$\mathcal{G}[\pi\mu^2]$	R (maxima)	$\mathcal{G}[\pi\mu^2]$
$\{a = 0.0$	3.84	$-2.484 \cdot 10^{-5}$	7.02	$-2.978 \cdot 10^{-5}$
	10.18	$-3.270 \cdot 10^{-5}$	13.33	$-3.479 \cdot 10^{-5}$
	73.1	$-4.785 \cdot 10^{-5}$	101.3	$-5.033 \cdot 10^{-5}$
$b = 0.1\}$	98.2	$-5.009 \cdot 10^{-5}$	208.1	$-5.583 \cdot 10^{-5}$
	5.13	-0.54496	8.48	-0.62000
	11.74	-0.66506	14.97	-0.69788
$\{a = 0.0$	18.18	-0.72371	97.3	-0.94062
	295.5	-1.08209	198.0	-1.03113